Nanoscale

PAPER

View Article Online
View Journal

Cite this: DOI: 10.1039/c5nr07503c

Nanosize effects assisted synthesis of the high pressure metastable phase in ZrO_2

Quanjun Li,[a] Huafang Zhang,[a] Ran Liu,[a] Bo Liu,[a] Dongmei Li,[a] Lirong Zheng,[b] Jing Liu,[b] Tian Cui[a] and Bingbing Liu*[a]

Received 27th October 2015,
Accepted 27th December 2015

DOI: 10.1039/c5nr07503c

www.rsc.org/nanoscale

The size effects on the high pressure behaviors of monoclinic (MI) ZrO_2 nanoparticles were studied using *in situ* high pressure synchrotron X-ray diffraction (XRD) and X-ray absorption spectroscopy (XAS). A size-dependent phase transition behavior under high pressure was found in nanoscale ZrO_2. The normal phase transition sequence of MI–orthorhombic I (OI)–orthorhombic II (OII) occurs in 100–300 nm ZrO_2 nanoparticles, while only the transition of MI–OI exists in ultrafine ~5 nm ZrO_2 nanoparticles up to the highest experimental pressure of ~52 GPa. This indicates that the size effects preclude the transition from the OI to the OII phase in ~5 nm nanoparticles. Upon decompression, the OII and OI phases are retained down to ambient pressure, respectively. This is the first observation of the pure OI phase ZrO_2 under ambient conditions. The bulk moduli of the MI ZrO_2 nanoparticles were determined to be B_0 = 192 (7) GPa for the 100–300 nm nanoparticles and B_0 = 218 (12) GPa for the ~5 nm nanoparticles. We suggest that the significant high surface energy precludes the transition from the OI to the OII phase and the nanosize effects enhance the incompressibility in the ultrafine ZrO_2 nanoparticles (~5 nm). Our study indicates that this is a potential way of preparing novel nanomaterials with high pressure structures using nanosize effects.

Introduction

ZrO_2 has attracted considerable attention because it is a hard material with excellent mechanical properties. Thus the crystal structures of ZrO_2 polymorphs have been extensively studied experimentally and theoretically under high pressure and/or at high temperatures.[1–6] The ambient temperature and pressure phase of ZrO_2 is a monoclinic baddeleyite structure (MI, space group: $P2_1/c$). With an increase of temperature, it transforms into a tetragonal (space group: $P4_2/nmc$) structure at temperatures above 1440 K,[7] and then to a cubic fluorite (space group: $Fm3m$) phase at very high temperatures (>2640 K).[8] Under high pressure, the MI phase transforms into an orthorhombic phase I (OI, space group: *Pbca*) at around 4.6 GPa, and then to an orthorhombic phase II (OII, space group: *Pnma*) at about 21 GPa.[6] The OI structure always coexists with the MI phase and the OII phase before it transforms completely into the OII phase upon compression, and it also coexists with the OII phase after release to ambient conditions.[1,2,5,6] Therefore, it is hard to obtain the pure OI phase ZrO_2 under ambient conditions, which precludes our understanding of this phase.

Recently, nanomaterials have been shown to have unique and enhanced properties, different from those of the corresponding bulk materials. Nanosize plays a critical role in enhancing the physicochemical properties of nanomaterials in general. A number of studies have indicated that unique phase transition sequences and elevated structural stabilities occur in some nanomaterials under high pressure.[4,9–14] The high pressure technique is likely to provide a potential route for preparing novel functional nanomaterials with excellent properties. For example, ultrahard nanotwinned cubic boron nitride has been synthesized from specially prepared BN precursor nanoparticles possessing onion-like nested structures at high temperatures and high pressure,[15] showing extremely high Vickers hardness, high oxidization temperature, and large fracture toughness. Subsequently, nanotwinned diamonds have been synthesized by high temperature and high pressure treatment of carbon onion nanoparticles,[16] and exhibit unprecedented hardness and thermal stability. Moreover, high pressure phase nanocrystals (nanowires, nanoparticles, and nanoporous rods), and amorphous nanomaterials have been found in several materials, such as TiO_2,[11,17–19] Y_2O_3,[20,21] PbTe,[12,22] and Ta_2O_5.[14] Pressure modified photoluminescence has been revealed in GaAs nanowires[23] and Ce-doped $Y_3Al_5O_{12}$ nanoceramics.[24] These reports have demonstrated that unique phase transition behaviors and physicochemical properties occur in nanomaterials under

[a]State Key Laboratory of Superhard Materials, Jilin University, Changchun 130012, P.R. China. E-mail: liubb@jlu.edu.cn; Tel: +86-431-85168256
[b]Beijing Synchrotron Radiation Facility, Institute of High Energy Physics, Chinese Academy of Sciences, Beijing 100049, China

high pressure. In addition, some reversible high pressure phases were found which can be obtained under ambient conditions in nanosized materials. This motivated us to study the size effects on the high pressure phase transitions in ZrO_2 and to explore a potential method for preparing the OI phase of ZrO_2.

In the present study we performed a high pressure investigation for ZrO_2 nanocrystals with different sizes using *in situ* XRD and XAS techniques. We found that the phase transitions in nanoscale ZrO_2 under high pressure are size-dependent. The different phase transition sequences MI–OI–OII and MI–OI occur in the coarser ZrO_2 nanoparticles and the ultrafine ~5 nm ZrO_2 nanoparticles upon compression, respectively. The OII and OI phases are retained down to ambient pressure in the two types of nanoparticles upon decompression, respectively. To our knowledge, this is the first study to obtain the pure OI phase of ZrO_2 under ambient conditions. These results indicate that the nanosize effects play important roles in the phase transition of ZrO_2.

Experiment

The ZrO_2 powders used in the experiments were synthesized by a similar hydrothermal method to that described in the previous report.[25] The samples were characterized using high resolution transmission electron microscopy (HRTEM) (JEOL JEM-3010). High pressure XRD experiments were performed using a diamond-anvil cell (DAC) with 300 μm diameter culets. A preindented stainless steel gasket drilled with a ~100 μm hole was used as the sample chamber. The samples and several small ruby balls were loaded in the chamber with a 4 : 1 methanol–ethanol mixture as the pressure-transmitting medium. *In situ* angle-dispersive synchrotron XRD measurements under high pressure for the ZrO_2 nanoparticles with a diameter of 100–300 nm were carried out at the 4W2 beamline of the Beijing Synchrotron Radiation Facility (BSRF). The incident wavelength of the monochromatic beam was 0.6199 Å. *In situ* angle-dispersive synchrotron XRD measurements under high pressure for the ZrO_2 nanoparticles with a size near ~5 nm were conducted at the X17C beamline of Brookhaven National Laboratory with a wavelength of 0.4066 Å. Rietveld refinements of the XRD patterns were performed using the GSAS program.[26] The XAS measurements at the Zr K edge (17.9976 keV) under various pressures were performed at the beamline 1W2B of BSRF. The powdered sample and amorphous boron powder as the pressure medium were mixed and sealed inside the DAC. The pressures in all experiments were determined by the standard ruby fluorescence method.

Results and discussion

The nanosize effects of ZrO_2 on its high pressure phase transitions were studied by two typical samples with particle sizes of 100–300 nm and ~5 nm. Fig. 1 shows representative TEM and HRTEM images of the two samples. As shown in Fig. 1a, the sample with the larger particles shows an irregular morphology with particle sizes in the range of 100–300 nm. The sample with the smaller particles exhibits a more uniform particle size of ~5 nm (Fig. 1b). The HRTEM images for the coarse nanoparticles (Fig. 1c) and the ultrafine nanoparticles (Fig. 1d) indicate that the two samples both consist of single crystalline nanoparticles with baddeleyite structures. These samples would provide supplementary information on the size effects on the high pressure phase transitions of ZrO_2 materials.

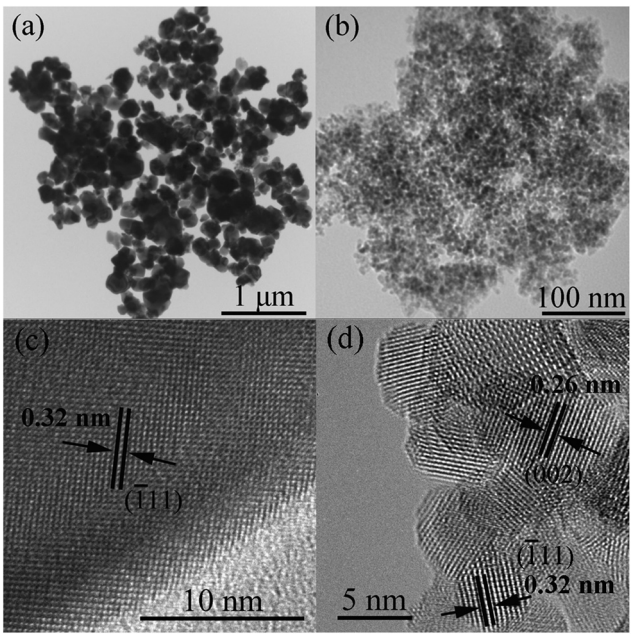

Fig. 1 TEM and HRTEM images of ZrO_2 nanoparticles with different sizes: (a and c) 100–300 nm and (b and d) ~5 nm.

A selection of XRD patterns representing the entire pressure range is shown in Fig. 2. As shown in Fig. 2, the starting phase

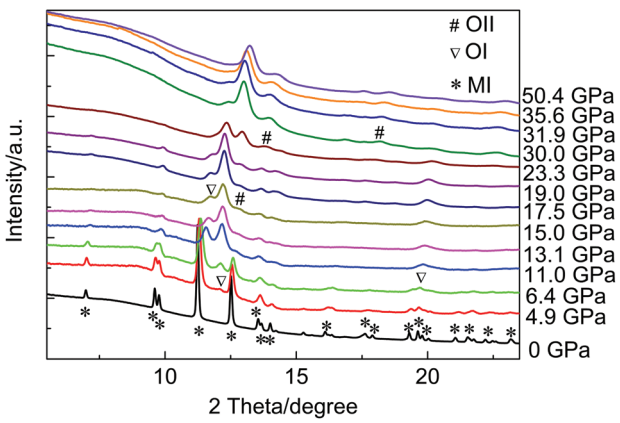

Fig. 2 High pressure XRD patterns of the 100–300 nm ZrO_2 nanoparticles.

of the larger ZrO_2 nanoparticles is the baddeleyite structure (MI, monoclinic, space group: $P2_1/c$). It is obvious that all XRD peaks shift to lower *d*-spacings upon compression, indicating a pressure-induced lattice contraction. At ~4.9 GPa, the sample starts a phase transformation from MI to an orthorhombic I (OI, orthorhombic, space group: *Pbca*) structure. The intensities of the OI peaks increase and those of the MI peaks decrease with increasing pressure. At ~15 GPa, a new peak of the orthorhombic II (OII, orthorhombic, space group: *Pnma*) phase occurs. At higher pressures (P > 17.5 GPa), the starting MI phase disappeared completely. The OI and OII phases coexist up to ~32 GPa and then completely transform into a single OII structure above ~35 GPa. After this, no further phase transition takes place up to the highest pressure (~50 GPa) that was applied. Fig. 3 shows the results of the Rietveld refinement assuming the cotunnite structure for the (OII) ZrO_2. Table 1 gives the refined parameters for the data under the highest pressure of 50.4 GPa and ambient conditions (released from 50.4 GPa). It is clear that both these XRD patterns are in good agreement with that of the OII phase. The OII phase remains stable down to ambient conditions, in agreement with those of previous reports.[2,27]

Fig. 4 shows XRD patterns obtained under pressure for the ~5 nm ZrO_2 nanoparticles. Under ambient conditions, the MI ZrO_2 nanoparticles (~5 nm) displayed an obvious size-induced broadening of their XRD peaks. A phase transformation from MI to OI starts at ~4.6–6.2 GPa. A precise determination of the onset transition pressure is not possible because of the merger of the XRD peaks. Above 16.2 GPa, the MI phase transforms completely into the OI phase. The transition pressure from MI to OI is similar to that for the larger ZrO_2 nanoparticles. However, the OI phase remains stable up to the highest pressure (~52 GPa) applied. This is different from what was observed for the larger ZrO_2 nanoparticles in which the OI phase transforms into the OII structure above 15 GPa. The nanosize thus effectively improves the structural stability of the OI phase in ZrO_2. Fig. 5 shows the results of the Rietveld refinement and Table 2 gives the refined parameters assuming the *Pbca* phase for (OI) ZrO_2. Obviously, the XRD patterns for both the high pressure phase and the decompressed material

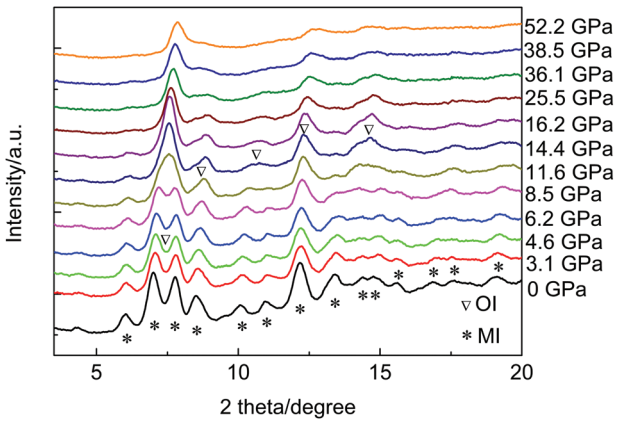

Fig. 4 High pressure XRD patterns for the ~5 nm ZrO_2 nanoparticles.

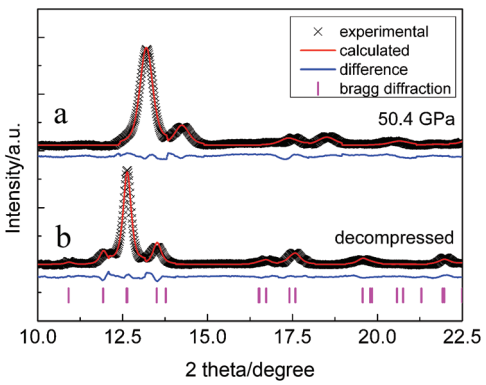

Fig. 3 XRD patterns and their Rietveld refinements for the ZrO_2 nanoparticles (100–300 nm) at different pressures. (a) 50.4 GPa; (b) quenched to ambient conditions from 50.4 GPa.

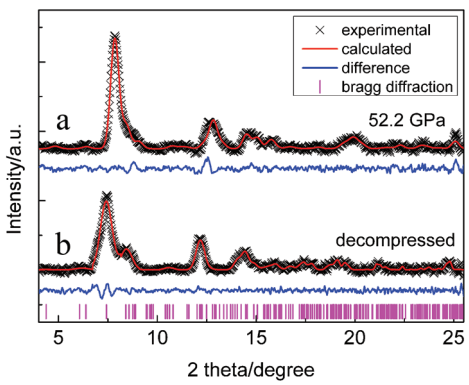

Fig. 5 XRD patterns and their Rietveld refinements for the ZrO_2 nanoparticles (~5 nm) at different pressures. (a) 52.2 GPa; (b) quenched to ambient conditions from 52.2 GPa.

Table 1 Parameters obtained from the Rietveld refinement of the XRD patterns of the OII phase of ZrO_2 at different pressures (100–300 nm nanoparticles). R_{wp} and R_p are the weighted profile *R*-factor and the profile *R*-factor, respectively

Pressure	*a*	*b*	*c*	*V*	R_{wp} (%)	R_p (%)
50.4 GPa	5.395	3.141	6.235	105.65	0.50	0.36
0 GPa	5.577	3.325	6.482	120.20	0.69	0.43

Table 2 Parameters obtained from the Rietveld refinement of the XRD patterns for the OI phase of ZrO_2 at different pressures (~5 nm nanoparticles)

Pressure	*a*	*b*	*c*	*V*	R_{wp} (%)	R_p (%)
52.2 GPa	9.162	5.264	4.919	237.24	0.69	0.51
0 GPa	10.152	5.271	5.162	276.22	0.65	0.47

agree well with that for the OI phase. Our results for the structural parameters of ZrO_2 are in accordance with that of Ozturk's result.[27] The OI phase was quenched from the high pressure, which indicates that the phase transition from MI to OI is also irreversible.

The pressure–volume data for ZrO_2 nanoparticles with different sizes are shown in Fig. 6. For the same MI phase we obtained bulk modulus B_0 = 192 (7) GPa for the coarser nanoparticles and B_0 = 218 (12) GPa for ultrafine nanoparticles from a fit to the Birch–Murnaghan equation of the state, in both cases with a fixed first order pressure derivative B'_0 = 4. The bulk modulus obtained for the ~5 nm nanoparticles is about 14% larger than that of the 100–300 nm nanoparticles. Obviously, the smaller grain size gives a lower compressibility for the MI phase of ZrO_2. This indicates that the nanosize effects play important roles in the compressibility of ZrO_2. The bulk moduli for the OI and OII phases are not given because reliable refinements could not be obtained due to the dramatic broadening, mixing or merging of the XRD peaks of the two phases under high pressure.

To further confirm the distinct phase transitions between the coarser nanoparticles and the small nanoparticles in ZrO_2, high pressure XAS studies were conducted. As shown in Fig. 7, the Fourier transformed spectra for both samples exhibit two intense peaks at about 1.7 and 3.2 Å (R–Δ) for the monoclinic structure at low pressures, corresponding to the phase-shift corrected values of about 2.2 and 3.5 Å respectively. These peaks represent the Zr–O and Zr–Zr distances. This agrees well with those of previous reports.[28,29] The peaks of ~5 nm nanoparticles are broader than those of the coarse nanoparticles, indicating the more various bond distances on the surface of ultrafine nanoparticles where three-dimensional periodicity disappears. For the coarse nanoparticles, the Zr–O bond distance decreases gradually upon compression (Fig. 7a), indicating the shrinkage of the polyhedron. However, the Zr–Zr distance shows little change at first, and then is divided into two separate peaks above ~16 GPa. The two peaks of 2.6 and 3.4 Å correspond to the Zr–Zr and Zr–O distances of the OII phase. This indicates that the OII phase starts to form. In addition, the released sample exhibits a similar spectrum with that of the OII structure, demonstrating the irreversible phase transition. Fig. 7b shows the different phase transition processes for the ultrafine nanoparticles, in which there is no separation for the Zr–Zr peak upon compression. The released sample shows a similar spectrum with that of the OI structure. These results are different from those of the coarse ZrO_2 nanoparticles. Although it is difficult to distinguish the phase transition pressure for these phase transitions by the XAS results, the quenched OI phase and OII phase in the ultrafine nanoparticles and coarse nanoparticles are clearly demonstrated, respectively. This is consistent with the XRD results.

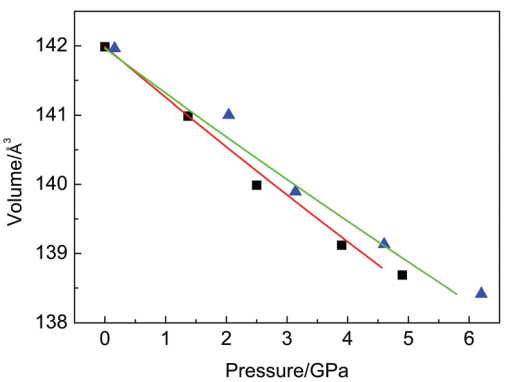

Fig. 6 Pressure–volume diagram of the MI phase of ZrO_2 nanoparticles with sizes of 100–300 nm (squares) and ~5 nm (triangles).

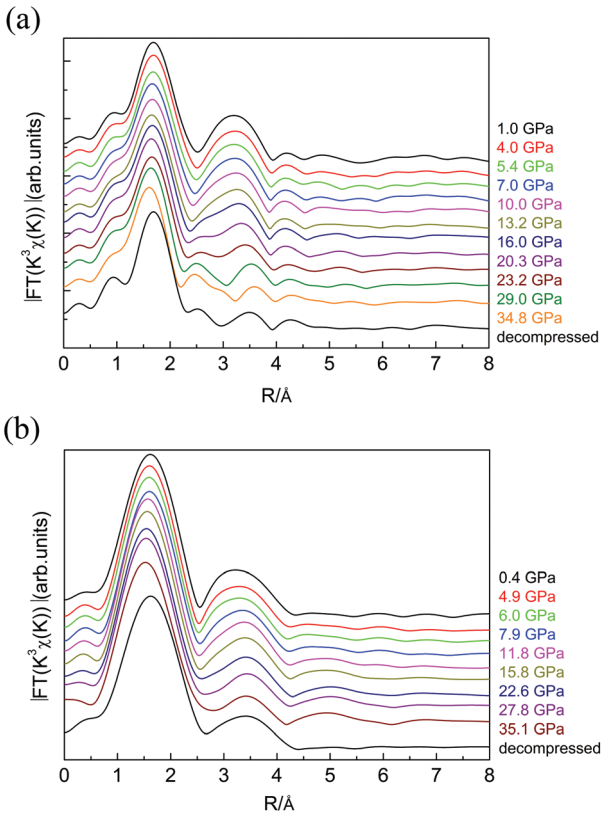

Fig. 7 Fourier transform moduli of the XAFS for the 100–300 nm ZrO_2 nanoparticles (a) and ~5 nm ZrO_2 nanoparticles (b) at high pressures.

Compared with bulk materials, nanomaterials show unique phase transition sequences and stabilities under high pressure because of size effects. It is known that the difference in surface energy between the high and low pressure phases influences the thermodynamics and kinetics of solid–solid phase transitions in nanocrystals. Size-dependent phase transition pressures have been found in various nanoparticles. Some nanocrystals (ZnO,[30] ZnS[9] and SnO_2 [31]) show enhanced transition pressures compared with the corresponding bulk materials. On the contrary, a transition pressure which decreases with decreasing grain size was found in Fe_2O_3 nanoparticles.[32] In addition, size-dependent phase transition sequences have been revealed in several nanoparticles (TiO_2,[17,19] Y_2O_3,[20] PbTe,[12] and so on). In our case, the normal

phase transition sequence of MI–OI–OII was found in 100–300 nm ZrO_2 nanoparticles, while only the MI–OI transition was found in ~5 nm ZrO_2 nanoparticles. The OII phase does not occur in ~5 nm nanoparticles up to the highest experimental pressure of 52.2 GPa, far higher than the transition pressure (~15 GPa) from the OI to the OII phase in coarser nanoparticles and in the bulk material. Generally, the surface energy of nanoparticles increases quickly with decreasing particle size. The high surface energy of nanoparticles leads to enhanced transition pressure in most materials. Although the transition pressure MI–OI does not show an obvious enhancement, the OI phase is stable up to ~52.2 GPa without any further phase transition. Thus, we suggest that the ultrahigh structural stability of the OI phase mainly derives from the high surface energy of the ultrafine ZrO_2 nanocrystals. A high energy kinetic hindrance thus exists for the phase transition OI–OII due to the size effects, which is most likely to result in an enhanced structural stability of the OI phase over a wide range of pressures and even preclude the transition from OI to OII under higher pressure. These results are distinctly different from the selective phase transition and pressure-induced amorphization observed in other nanomaterials.[10–14,17–22] Our study further demonstrates that the high surface energy of nanomaterials can modify the phase transition sequences and phase stability.

It is worth noting that OII-ZrO_2 was predicted to have a low mechanical hardness compared to MI and OI. The low mechanical strength was explained by the increase in the shortest Zr–O bond length in the OII phase.[6] The hardness trend of ZrO_2 phases is thus OII < MI < OI.[6] Therefore, the OII phase is not an ideal structure for improving the mechanical hardness of ZrO_2. Instead, the OI phase is the more ideal one. Unfortunately, the OI phase usually coexists with the MI and OII phases in a broad pressure range which makes it difficult to obtain the pure OI structure. It is interesting that the OI phase is successfully obtained in ~5 nm ZrO_2 nanoparticles in our case. The OI phase exists in a large pressure range of 16–52 GPa and can be quenched to ambient conditions. This provides a new method for preparing OI phase ZrO_2 nanoparticles which may have excellent mechanical hardness.

Conclusions

In summary, we studied the high pressure phase transitions of ZrO_2 nanoparticles using *in situ* synchrotron XRD and XAS techniques. A size-dependent phase transition under high pressure was found in nanoscale ZrO_2. The MI phase starts to transform into the OI phase at ~4.9 GPa and then to the OII structure at ~15 GPa in 100–300 nm size ZrO_2 nanoparticles. In contrast, in ~5 nm ZrO_2 nanoparticles the OI phase occurs at 4.6–6.2 GPa and remains stable up to the highest experimental pressure of ~52 GPa. Upon decompression, the OII and OI phases are retained down to ambient pressure in the two types of nanoparticles, respectively. This is the first observation of single OI phase ZrO_2 under ambient conditions. The bulk modulus of the MI ZrO_2 nanoparticles was determined to be B_0 = 192 (7) GPa for the 100–300 nm nanoparticles and B_0 = 218 (12) GPa for the ~5 nm nanoparticles. These results indicate that the nanosize effects play important roles in the phase transition behaviors and compressibility of ZrO_2. We suggest that the high surface energy precludes the transition from the OI to the OII phase and the nanosize effects enhance the bulk modulus of the ultrafine ZrO_2 nanoparticles (~5 nm).

Acknowledgements

This work was financially supported by the NSFC (51320105007, 51032001, 21073071, and 11374120), Program for Changjiang Scholars and Innovative Research Team in University (No. IRT1132), and the Cheung Kong Scholars Programme of China.

Notes and references

1 J. M. Leger, P. E. Tomaszewski, A. Atouf and A. S. Pereira, *Phys. Rev. B: Condens. Matter*, 1993, **47**, 14075–14083.
2 S. Desgreniers and K. Lagarec, *Phys. Rev. B: Condens. Matter*, 1999, **59**, 8467–8472.
3 M. Sternik and K. Parlinski, *J. Chem. Phys.*, 2005, **122**, 064707.
4 F. X. Zhang, M. Lang, R. C. Ewing, J. Lian and Z. W. Wang, *J. Phys. Chem. C*, 2009, **113**, 14658–14662.
5 O. Ohtaka, H. Fukui, T. Kunisada, T. Fujisawa, K. Funakoshi, W. Utsumi, T. Irifune, K. Kuroda and T. Kikegawa, *Phys. Rev. B: Condens. Matter*, 2001, **63**, 174108.
6 Y. Al-Khatatbeh, K. K. M. Lee and B. Kiefer, *Phys. Rev. B: Condens. Matter*, 2010, **81**, 214102.
7 P. Aldebert and J. P. Traverse, *J. Am. Ceram. Soc.*, 1985, **68**, 34–40.
8 D. K. Smith and C. F. Cline, *J. Am. Ceram. Soc.*, 1962, **45**, 249–250.
9 Z. W. Wang, L. L. Daemen, Y. S. Zhao, C. S. Zha, R. T. Downs, X. D. Wang, Z. L. Wang and R. Hemley, *Nat. Mater.*, 2005, **13**, 1–6.
10 V. Swamy, A. Y. Kuznetsov, L. S. Dubrovinsky, A. Kurnosov and V. B. Prakapenka, *Phys. Rev. Lett.*, 2009, **103**, 075505.
11 Q. J. Li, B. B. Liu, L. Wang, D. M. Li, R. Liu, B. Zou, T. Cui, G. T. Zou, Y. Meng, H. K. Mao, Z. X. Liu, J. Liu and J. X. Li, *J. Phys. Chem. Lett.*, 2010, **1**, 309–314.
12 Z. W. Quan, Z. P. Luo, Y. X. Wang, H. W. Xu, C. Y. Wang, Z. W. Wang and J. Y. Fang, *Nano Lett.*, 2013, **13**, 3729–3735.
13 D. Machon, L. Piot, D. Hapiuk, B. Masenelli, F. Demoisson, R. Piolet, M. Ariane, S. Mishra, S. Daniele, M. Hosni, N. Jouini, S. Farhat and P. Melinon, *Nano Lett.*, 2014, **14**, 269–276.
14 X. J. Lv, Q. Y. Hu, W. G. Yang, L. G. Bai, H. Sheng, L. Wang, F. Q. Huang, J. G. Wen, D. J. Miller and Y. S. Zhao, *J. Am. Chem. Soc.*, 2013, **135**, 13947–13953.

15 Y. J. Tian, B. Xu, D. L. Yu, Y. M. Ma, Y. B. Wang, Y. B. Jiang, W. T. Hu, C. C. Tang, Y. G. Gao, K. Luo, Z. S. Zhao, L. M. Wang, B. Wen, J. L. He and Z. Y. Liu, *Nature*, 2013, **493**, 385–388.
16 Q. Huang, D. L. Yu, B. Xu, W. T. Hu, Y. M. Ma, Y. B. Wang, Z. S. Zhao, B. Wen, J. L. He, Z. Y. Liu and Y. J. Tian, *Nature*, 2014, **510**, 250–253.
17 V. Swamy, A. Kuznetsov, L. S. Dubrovinsky, P. F. McMillan, V. B. Prakapenka, G. Shen and B. C. Muddle, *Phys. Rev. Lett.*, 2006, **96**, 135702.
18 V. Pischedda, G. R. Hearne, A. M. Dawe and J. E. Lowther, *Phys. Rev. Lett.*, 2006, **96**, 035509.
19 G. R. Hearne, J. Zhao, A. M. Dawe, V. Pischedda, M. Maaza, M. K. Nieuwoudt, P. Kibasomba, O. Nemraoui, J. D. Comins and M. J. Witcomb, *Phys. Rev. B: Condens. Matter*, 2004, **70**, 134102.
20 L. Wang, W. G. Yang, Y. Ding, Y. Ren, S. G. Xiao, B. B. Liu, S. V. Sinogeikin, Y. Meng, D. J. Gosztola, G. Y. Shen, R. J. Hemley, W. L. Mao and H. K. Mao, *Phys. Rev. Lett.*, 2010, **105**, 095701.
21 L. Piot, S. L. Floch, T. Cornier, S. Daniele and D. Machon, *J. Phys. Chem. C*, 2013, **117**, 11133–11140.
22 Z. W. Quan, Y. X. Wang, I. T. Bae, W. S. Loc, C. Y. Wang, Z. W. Wang and J. Y. Fang, *Nano Lett.*, 2011, **11**, 5531–5536.
23 I. Zardo, S. Yazji, C. Marini, E. Uccelli, A. F. Morral, G. Abstreiter and P. Postorino, *ACS Nano*, 2012, **6**, 3284–3291.
24 A. Podhorodecki, P. Gluchowski, G. Zatryb, M. Syperek, J. Misiewicz, W. Lojkowski and W. Strek, *J. Am. Ceram. Soc.*, 2011, **94**, 2135–2140.
25 W. Z. Li, H. Huang, H. J. Li, W. Zhang and H. C. Liu, *Langmuir*, 2008, **24**, 8358–8366.
26 B. H. Toby, *J. Appl. Crystallogr.*, 2001, **34**, 210–213.
27 H. Ozturk and M. Durandurdu, *Phys. Rev. B: Condens. Matter*, 2009, **79**, 134111.
28 A. Yoshiasa, H. Arima, M. Okube, H. Fukui, A. Nakatsuka, Y. Katayama and O. Ohtaka, *J. Phys.: Conf. Ser.*, 2009, **190**, 012119.
29 C. Degueldre and K. Dardenne, *Nucl. Instrum. Methods Phys. Res., Sect. B*, 2005, **238**, 323–328.
30 L. H. Wang, H. Z. Liu, J. Qian, W. G. Yang and Y. S. Zhao, *J. Phys. Chem. C*, 2012, **116**, 2074–2079.
31 Y. He, J. F. Liu, W. Chen, Y. Wang, H. Wang, Y. W. Zeng, G. Q. Zhang, L. N. Wang, J. Liu, T. D. Hu, H. Hahn, H. Gleiter and J. Z. Jiang, *Phys. Rev. B: Condens. Matter*, 2005, **72**, 212102.
32 Z. W. Wang, S. K. Saxena, V. Pischedda, H. P. Liermann and C. S. Zha, *Phys. Rev. B: Condens. Matter*, 2001, **64**, 012102.

